Journal of Metals, Materials and Minerals, Vol.25 No.2 pp.57-70, 2015

Microstructure Based Finite Element Simulation of JCO Forming Process for Pipeline X65

Wut THIANNGOEN, Saranya KINGKLANG and Vitoon UTHAISANGSUK*

Department of Mechanical Engineering, Faculty of Engineering,
King Mongkut's University Technology Thonburi,
126 Pracha Uthit Road, Bang Mod, Thung Khru, Bangkok 10140, Thailand

Abstract

In recent years, strong increases in energy demand have become the most important issue in every section. High strength pipeline steels make large contribution to cost reduction for fuel transportation in oil and gas industries due to their great combination of optimal strength and toughness properties. Mechanical properties of pipeline steel tubes are significantly influenced by their microstructure characteristics, which in turn are controlled by the production. In this work, the JCO forming process of gas pipeline tube made of hot–rolled steel grade X65with ferrite/pearlite microstructure was investigated by means of a FE multi–scale modeling approach. Three different scales including the nano–scale of a ferrite–cementite bi-lamella of pearlite, pearlite/ferrite microstructure on the micro–scale and macro–scale tube were considered. Firstly, local mechanical properties of the X65 steel were examined, in which steel specimens were heated up to austenitization temperature and cooled down to room temperature with high and low cooling rate. Obtained microstructures from both conditions represented material in the center and at the skin of the tube. Stress–strain responses of both different zones were determined by tensile test. Subsequently, FE representative volume element (RVE) models were generated taking into account existing phases and morphologies. Effective flow stress curve of pearlite was predicted by the nano–scale model. In the micro–scale RVE, pearlite with different morphologies distributed in a ferritic matrix was modeled. It was found that stress–strain curve of the X65 steel described by the micro–scale model agreed well with experimental flow curve. Then, two FE simulations of the JCO forming were carried out, by which one was defined with the same microstructure for all area of the tube and other incorporated different microstructures for the skin and center area of the tube. Obviously, the most critical stresses on the formed tube calculated by both models were deviated. Finally, RVE simulations were carried out for the skin and center area of the tube subjected to the JCO forming process. Stress and strain distribution in the microstructure of the X65 steel tube could be evaluated and discussed.

Keywords : X65 pipeline steel, Multi-scale modeling, RVE, FE simulation

DOI : 10.14456/jmmm.2015.16

Introduction

Nowadays, global energy demand has rapidly risen from year to year. Natural gas is mostly used as energy source in Thailand and it is predicted that its usage will be increased up to 39% in the future. High amount of natural gas is used for power generation, fuel in industries and raw materials for chemical industries. Applications of natural gas in Thailand are fuel in industries, transportation, raw materials for chemical industries and especially up to 59% of produced natural gas is taken for power generation. It was reported that 79% of the overall natural gas in Thailand is produced in the country.(1) Generally, natural gas must be transported to production plants and sub–stations by long distance pipeline on ground or under seawater. To reduce cost of oil and gas transportation, special high strength steel grades haven been widely used for the pipelines. High strength and optimum toughness are the most common requirements of pipeline steels. Mechanical properties and fracture behavior of pipeline steel tubes are influenced by their microstructure characteristics, which are controlled by the production process.(5) Thus, better understanding of mechanical behavior of pipeline steels and pipeline tubes after forming is necessary, by which production process parameters should be taken into account. By this manner, pipelines under applications could be more accurately investigated and subsequently optimized.

*Corresponding author E-mail : vitoon.uth@kmutt.ac.th

Microstructures of two pipeline steels grade X52 and X65 were examined by *Wang et al.*[2] It was found that morphologies of developed pearlite in these steels depended on different pearlite formation mechanisms including the traditional manner of nucleation at ferrite–austenite interfaces, formation of carbides at ferrite-ferrite grain boundaries, formation of carbides at ferrite–austenite interfaces, and growth and branching of carbides at ferrite/ferrite grain boundaries. Internal stress evolutions of ferrite–pearlite steels under plastic deformation were examined by *Allain et al.*[3] Significant strain incompatibility between ferrite and pearlite was observed as large internal stresses were generated in pearlite during overall strain. Furthermore, mechanical properties of the steels were affected by lamella spacing of pearlite. It was stated that for pearlitic structure, increasing flow stress due to strain hardening was not depended on inter–lamellar spacing, but only on plastic strain. *Lascher et al.*[4] calculated effective macroscopic stress–strain curve of a ferrite–pearlite pipeline steel tube by using a multi scale approach based on the homogenization method. A model for ferrite–cementite bi–lamella structure of pearlite was used to calculate effective mechanical behavior of the pearlitic phase. In case of cementite, it was shown that both elastic and plastic properties were anisotropic. Thus, anisotropy behavior of each phase in the pearlitic steel tube was considered in a representative volume element (RVE). Anisotropy of ferrite was defined due to that the ferritic matrix exhibited smaller grain sizes in the transverse direction to the rolling direction. Finally, macroscopic stress–strain curve of the pipeline steel could be predicted with regards to its microstructure characteristics.

U– and O– forming steps by production of gas pipeline steel tube were simulated by *Laschet et al.*[5] A nano–scale model of ferrite–cementite bi–lamella structure in pearlite and a two phase ferrite/pearlite microstructure model were introduced by using RVE technique. Individual anisotropic elasto–plastic stress–strain curves of each phase constituents were applied to predict overall flow stress of X65 steel pipe. It was found that microstructure of tube surface exhibited slightly less pearlite content, reduced lamella spacing and lower residual dislocation density than that of tube center. Thus, different flow curves were defined for both regions and then applied for FE simulation of the U– and O–forming process. Finally, the most critical local stresses and strains of the pipeline steel tube after the O–forming were predicted. A pipeline forming process was investigated by *Palumbo et al.*[6] In this work, tube forming included forming of longitudinal border of steel blank (C–forming), air bending of the C–formed blank (U–bending) and forming inside a circular shaped die of the U–formed blank (O–forming). FE simulations of all subsequent forming steps were carried out. Stress and strain states in the tube during each forming procedure were investigated. Effects of each forming step on tube section end profiles and on tube lengthwise inflection were evaluated. A strong influence on the tube shape was observed by the C–forming step. A complete UOE pipe forming process of X80 steel grade was numerically analyzed by *Ren et al.*[7] that incorporated crimping, U–forming, O–forming, joining, welding and expanding. A kinematic hardening model was taken into account to describe Bauschinger effect under loading–reverse loading deformation. Hereby, open seam distance could be very well predicted. The U–shaped plate was subjected to bending and reverses bending during the O–forming step. Springback of the reverse bending section tended to narrow open–seam, while springback of the crimping tended to enlarge open–seam. A good lubrication was helpful for high–quality pipes. *Liu et al.*[8] investigated failure of natural gas buried X65 steel pipeline under deflection load. Strain softening properties of pipeline after plastic collapse were simulated, in which effects of soil types and model sizes on the maximum deflection displacement were considered. Based on this method, the maximum deflection displacement of pipeline was calculated and an effective engineering criterion for the safety performance was introduced.

It could be seen that from production to application of high strength pipeline steels are subjected to various complex heat treatment cycles and mechanical loadings. Thus, in this work, a microstructure based FE multi–scale approach was applied to investigate effects of the JCO forming on a gas pipeline tube made of hot–rolled steel grade X65. Austenitizing with following medium and low cooling rate was performed for the X65 pipeline steel, in which obtained microstructures from each condition approximately represented material in the center and at the skin of the tube. Stress–strain responses of both different zones could be thus determined by tensile test. Three different scales including the nano–scale of a ferrite–cementite bi–lamella structure in pearlite, pearlite/ferrite microstructure on the micro–scale and macro–scale tube were considered. RVE models were generated taking into account existing phases and morphologies, which were characterized by optical and scanning electron microscope. Effective flow stress curve of

pearlite was determined by the nano–scale model composed of a ferrite and cementite lamellae. In the micro–scale RVE, pearlite with different morphologies distributed in a ferritic matrix was modeled. Then, two FE simulations of the JCO forming were carried out, by which one was defined with the same microstructure for all area of the tube and other incorporated different microstructures for the skin and center area of the tube. Finally, micro–scale RVE simulations were carried out for the skin and center area of the tube subjected to the JCO forming process in order to evaluate stress and strain distribution in the microstructure of the X65 steel tube.

Materials and Experimental Procedures

In this work, a pipeline tube of the steel grade X65 grade that was produced by JCO forming process and had an outer diameter of 28 inch and a thickness 0.874 inch. It was used to verify stress–strain responses calculated by the microstructure based approach. Furthermore, hot–rolled steel plate grade S450J0, which was comparable to the X65 steel plate according to EN 10025–2 standard, were taken to determine material parameters for RVE FE simulations. Chemical compositions of the investigated X65 pipeline steel tube and S450J0 steel plate were analyzed by optical emission spectrometer, as given in Table 1. It was found that the chemical composition of the X65 steel tube was similar to the S450J0 hot–rolled plate. It was reported[4,5] that pipeline steel tube exhibited different ferritic/pearlitic microstructure characteristics at the skin and center area of the tube, since materials in both locations of a thick plate were subjected to unlike cooling rates. Therefore, in this work the S450J0 steel plates were used to generate these microstructures of both zones by applying two heating and subsequent cooling procedures. Initially, steel plates were heated up to the temperature of 950ºC and held for 20 minutes in order to obtain a homogeneous austenitic structure. Then, the plates were cooled down to room temperature under two atmospheres, namely, in air and in furnace, which represented cooling condition of surface and center region of the tube, respectively. Subsequently, for characterizing occurred microstructure, steel plates after heat treatments were grinded and mechanically polished. Hereby, a solution of nitric acid with 3% concentrate was used as etchant. Micrographs of the steel plates from each cooling conditions were taken by optical microscope (OM) and scanning electron microscope (SEM) and microstructure parameters for example, grain size, phase fraction and lamella spacing, required for the modeling were obtained. In addition, stress–strain responses of the steel plates were determined by tensile test of specimens taken steel plates from each condition. The tensile samples were prepared according to ASTM E8/E8M standard.

Table 1. Chemical composition of the investigated X65 pipeline tube and hot rolled steel grade S450J0 (in wt.%).

Material	C	Si	Mn	P	S	Cr	Nb	Ni	Al
Pipeline grade X65	0.095	0.279	1.505	0.010	0.002	0.012	0.043	0.003	0.013
S450J0	0.089	0.300	1.468	0.014	0.002	0.020	0.048	0.015	0.035

Micromechanical modeling

Definition of elastic behavior of pearlite on the nano–scale

Initially, a bi–lamella structure of pearlite, which consisted of cementite and ferrite in eutectoid pearlite with the volume fraction of V_c = 1/9 and V_f = 8/9, respectively was generated on the nano–scale.More details about the nano–scale RVE were given later by definition of elasto–plastic behavior of pearlite. Elastic properties of the bi–lamella pearlite in the center and at the surface were defined according to Hooke law as reported in [5]. The effective Hooke matrices (in GPa) for both zones are expressed in Eq. (1). It could be seen that the elastic behavior of the pearlite at the plate surface was slightly stuffer than that in the center.

$$C_{cent}^{eff} = \begin{vmatrix} 288.4 & 87.1 & 100.2 & 5.7 & -8.9 & -13.3 \\ & 279.0 & 114.5 & 13.7 & 15.7 & 0.7 \\ & & 269.9 & -19.0 & -7.4 & 11.7 \\ & & & 44.3 & -10.2 & 10.8 \\ & & & & 65.9 & -24.5 \\ & \text{SYM} & & & & 73.5 \end{vmatrix}$$

$$C_{skin}^{eff} = \begin{vmatrix} 288.7 & 88.9 & 99.4 & -8.7 & -9.4 & 15.8 \\ & 284.8 & 98.5 & -14.6 & 12.0 & -2.8 \\ & & 274.8 & 23.6 & -7.44 & -13.4 \\ & & & 50.7 & 15.3 & 11.6 \\ & & & & 70.3 & 26.5 \\ & \text{SYM} & & & & 69.5 \end{vmatrix} \quad (1)$$

Definition of elasto–plastic behavior of ferrite in pearlite

Ferrite in eutectoid pearlite was defined as isotropic material on the nano–scale. Its isotropic stress–strain behavior could be calculated according to the Gutierrez–Altuna physically based model[9], as given in Eq. (2).

$$\sigma_y = \sigma_0 + \Delta\sigma = \sigma_0 + \alpha MGb\sqrt{\rho} \quad (2)$$

Where the first term σ_0 represented the Peierls stress for dislocation movement that depended on the chemical composition of the examined steel[10] and the second term $\Delta\sigma$ described material strengthening by dislocation density evolution, as presented in Eq.(3) and Eq.(4), respectively.

$$\sigma_0 = 77 + 750(\%P) + 60(\%Si) + 80(\%Cu) + 45(\%Ni) + 60(\%Cr) + 80(\%Mn) + 11(\%Mo) + 5000(\%N_{SS}) \quad (3)$$

$$\Delta\sigma = \alpha M\mu b\sqrt{\frac{1}{bLk_2}\left[1 - \exp(-k_2 M\bar{\varepsilon}^{pl})\right] + \rho_0 \exp(-k_2 M\bar{\varepsilon}^{pl})} \quad (4)$$

Where α is a material constant (α = 0.33), M is the Taylor factor (M = 3), μ is the shear modulus (μ = 80,000 MPa), b is the Burgers vector (b = 2.5x10^{-10}m) and ρ_0 is the initial dislocation density. It was found that dislocation densities in ferrite lamella were higher than those in ferrite matrix.[11] A reduction of nearly 40% of dislocation density near free surfaces of thin sheets was calculated by *Keller et al.*[12] in comparison to the central region. Hence, in this work, an initial dislocation density of ρ_0 of 1x10^{13} was presumed for ferrite lamella in pearlite at the skins, while the value of 3x10^{13} was defined for that in the central microstructure. κ_2 is a factor representing recovery of dislocation and was defined as $10^{-5}/d_\alpha$, by which d_α was basically the ferritic grain size. L is the dislocation mean free path and equal to d_α. Note that lamella spacing of pearlite in the skin and in the central area of 6.25 μm and 16 μm, respectively, was determined for the examined steel by SEM. In this study, this lamella spacing was used as the dislocation mean free paths L. Thicker lamella, for example in the central region, exhibited larger L value. With regard to this model, stress–strain curves of the ferrite in pearlite were predicted for both zones, as depicted in Figure 1. It can be seen that at the beginning of deformation, flow stress of the central area was higher than that of the skin due to higher dislocation density. However, higher strain hardening was definitely observed for the surface region, because smaller lamella (lower κ_2 value) led to larger work hardening rate with respect to the Hall–Petch effect.

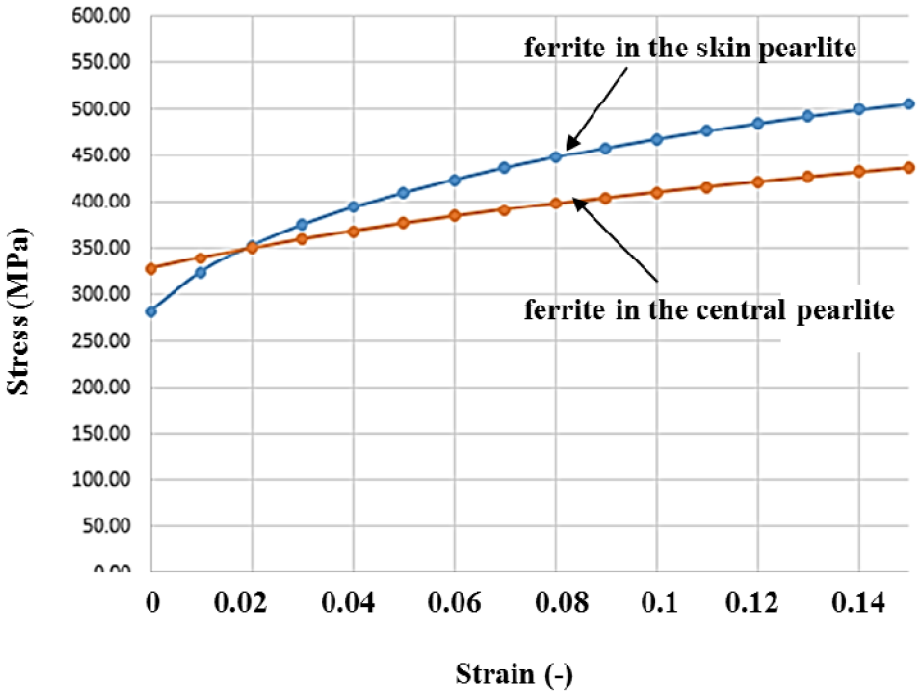

Figure 1. Calculated true stress–strain curves of the ferrite in pearlite of the examined steel.

Definition of elasto–plastic behavior of cementite in pearlite

It was stated that the hard and brittle cementite phase in pearlite showed some anisotropic elasticity and plasticity.(4) However, *Luque et al.*(5) performed nano–indentation tests on single cementite plate and found a mean tensile strength of about 4 GPa. By analyzing hysteresis area below force–displacement curves from the nano–indentation tests[13], it was found that plastic deformation done by cementite was nearly 40% of the ferrite one. Based on this consideration, plastic flow stress of cementite in pearlite could be described by Eq. (5), as shown in Figure 2. Hereby, the cementite exhibited a quasi–perfect plastic behavior with a small strain hardening. This stress–strain curve of cementite was used for pearlite in both zones.

$$\sigma = 4270\varepsilon^{0.0095} \tag{5}$$

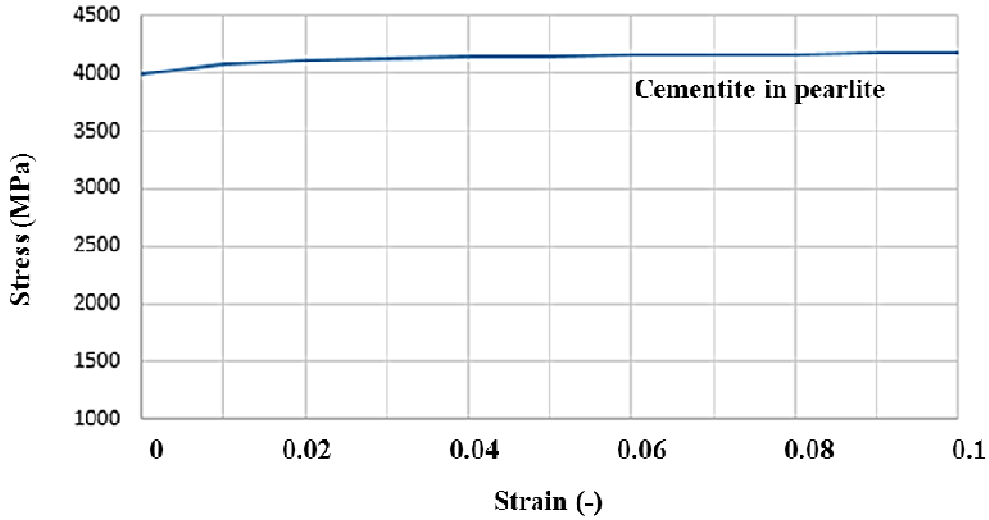

Figure 2. Modeled true stress–strain curves of the cementite in pearlite.

Moreover, the quadratic Hill's yield criterion was applied for representing anisotropic plastic behavior of the cementite, as expressed in Eq. (6).

$$F(\sigma)=\sqrt{F\left(\sigma_{yy}-\sigma_{zz}\right)^2+G\left(\sigma_{zz}-\sigma_{xx}\right)^2+H\left(\sigma_{xx}-\sigma_{yy}\right)^2+2L\tau_{yz}^2+2M\tau_{xz}^2 2N\tau_{xy}^2} \quad (6)$$

Where F, G, H, L, M, N are coefficients obtained by uniaxial tensile and shear tests. They are defined by the six anisotropic yield stress ratios, as provided in Eq.(7)

$$R_{xx}=\frac{\sigma_{xx}^{Y}}{\sigma_0};R_{yy}=\frac{\sigma_{yy}^{Y}}{\sigma_0};R_{zz}=\frac{\sigma_{zz}^{Y}}{\sigma_0};R_{xy}=\frac{\sigma_{xy}^{Y}}{\sigma_0};R_{xz}=\frac{\sigma_{xz}^{Y}}{\sigma_0};R_{yz}=\frac{\sigma_{yz}^{Y}}{\sigma_0} \quad (7)$$

It was assumed that the yield stress ratio is similar to the stiffness ratio in the corresponding direction. Thus, following stress ratios were taken for a polycrystalline cementite lamella.[5]

$$R_{xx}=1,\ R_{yy}=0.89,\ R_{zz}=0.83,\ R_{xy}=0.18,\ R_{xz}=0.7 \text{ and } R_{yz}=0.7 \quad (8)$$

Determination of effective flow stresses of pearlite

On the nano scale, the bi–lamella structure of pearlite was modeled by a two layer RVE, as shown in Figure 3a. The phase fractions of 1/9 and 8/9 were used for ferrite and cementite, respectively. In this work, two types of the bi–lamella RVE were investigated, namely, for the skin zone (high cooling rate) and for the central zone (low cooling rate). From SEM micrographs, lamella spacing of the skin and central zone of 6.25 μm and 16 μm were measured, as seen in Figure 3b. Virtual tensile tests in 3 principal directions (x, y and z) and virtual shear tests in other 3 directions (xy, xz and yz) were carried out for the modeled bi–lamella RVE. Effective stress–strain curves of the pearlite were obtained by averaging micro–stresses and equivalent plastic micro–strains, as depicted in Figure 4. It was observed that strain hardenings of pearlite in the skin region were larger than those in the central area for all directions. Additionally, higher equivalent stresses in x direction than other directions were predicted for both areas. For each effective flow stress, local stress ratios R were calculated by averaging stresses at selected plastic strains in the range of 0 to 0.12. The predicted stress ratios in all directions were summarized in Eq. (9) and (10). It can be seen that pearlite in the skin area showed a little lower anisotropy than that in the central area.

Skin pearlite: $R_{xx}=1,\ R_{yy}=0.99,\ R_{zz}=0.95,\ R_{xy}=0.96,\ R_{xz}=0.83$ and $R_{yz}=0.90$ (9)

Central pearlite: $R_{xx}=1,\ R_{yy}=0.95,\ R_{zz}=0.94,\ R_{xy}=0.93,\ R_{xz}=0.88$ and $R_{yz}=0.88$ (10)

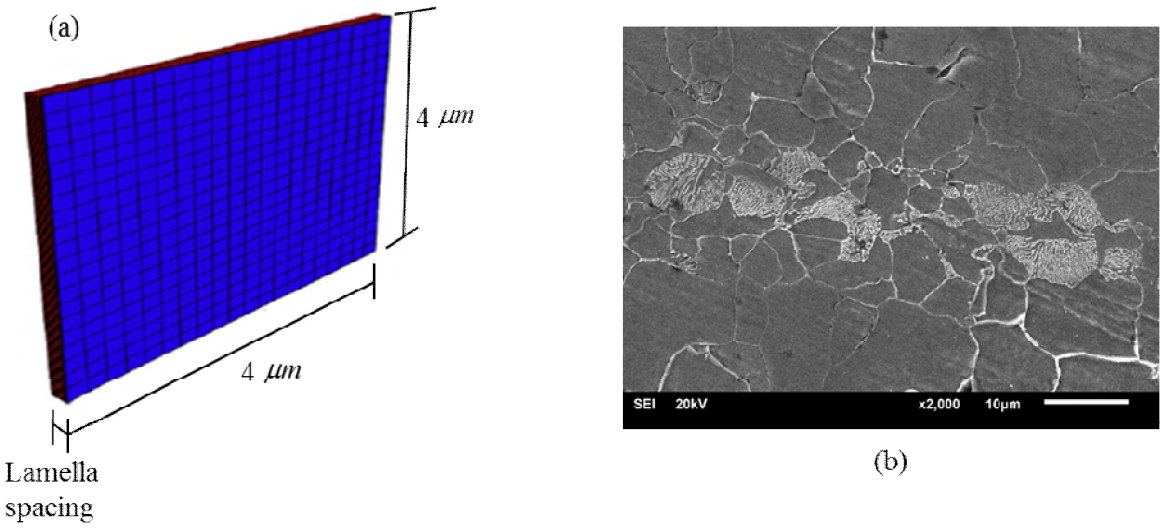

Figure 3. (a) Nano–scale RVE model for a bi–lamella structure of pearlite and (b) SEM micrograph of the investigated steel.

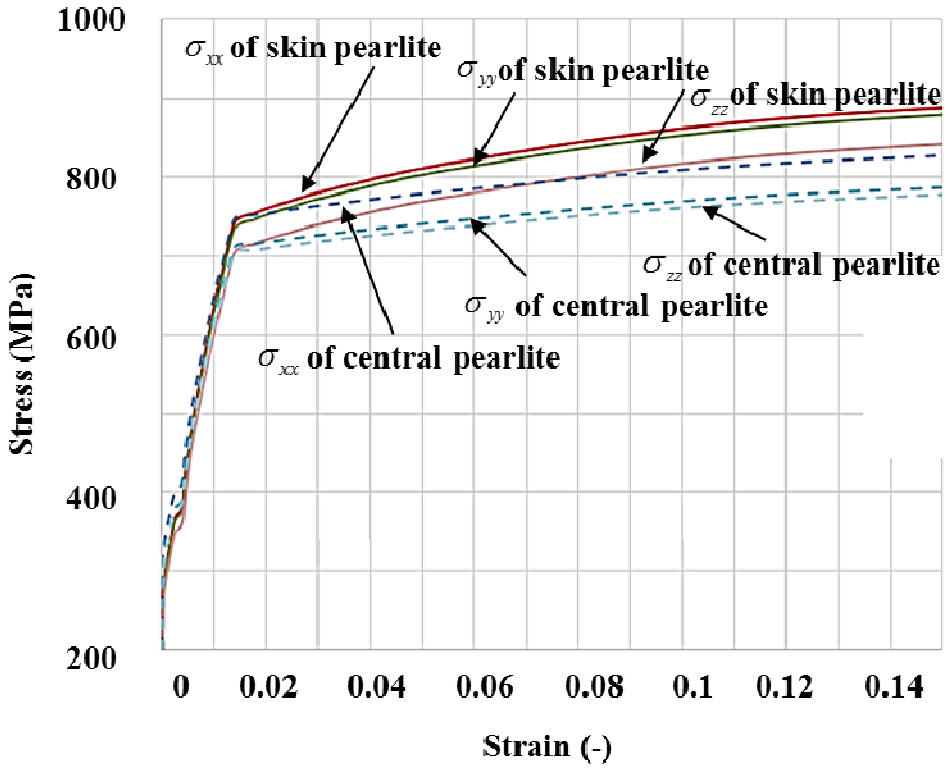

Figure 4. Determined stress–strain curves of pearlite in the skin (high cooling rate) and in the central (low cooling rate) area of the examined steel.

Definition of elasto–plastic behavior of ferrite matrix

To define anisotropic plastic behavior of the ferrite matrix, the Gutierrez–Altuna model was applied again, in which different dislocation mean free paths, which corresponded to the mean grain size, in the rolling and transverse direction of the ferrite matrix were taken into account. The mean grain sizes in the rolling and transverse direction of L_R = 11.86 mm, L_T = 6.85 mm and L_R = 13.10 mm, L_T = 7.56 mm were measured for the skin and central area, respectively. It was found that the central region showed microstructure with a larger ferritic grain size than the skin regions in all directions. Furthermore, different initial dislocation densities ρ_0 of $2.5 \cdot 10^{13}$ and $1.5 \cdot 10^{13}$ were defined for the ferrite matrix in the central and skin microstructure, respectively.[5] Calculated flow curves of the ferrite matrix in different zones and directions were depicted in Figure 5. It was seen that the skin region of the investigated steel exhibited higher flow stresses than the central region. This was due to higher C content in the ferrite matrix of the skin zone as a consequence of slightly lower amount of pearlite. On the other hand, the flow stresses in the transverse direction were higher than those in the rolling direction because of smaller grain size of microstructure in the transverse direction. Finally, the yield stress ratios for the ferrite matrix were calculated by assuming isotropy in the transverse plane *T–N* as following.

$$R_{RR} = 1,\ R_{TT} = \upsilon,\ R_{NN} = \upsilon,\ R_{RR} = 1,\ R_{RT} = 1,\ R_{RN} = 1 \text{ and } R_{TN} = \upsilon \tag{11}$$

Where $\upsilon = 1.0937$ for the center and $\upsilon = 1.0941$ for the skin were defined.[5]

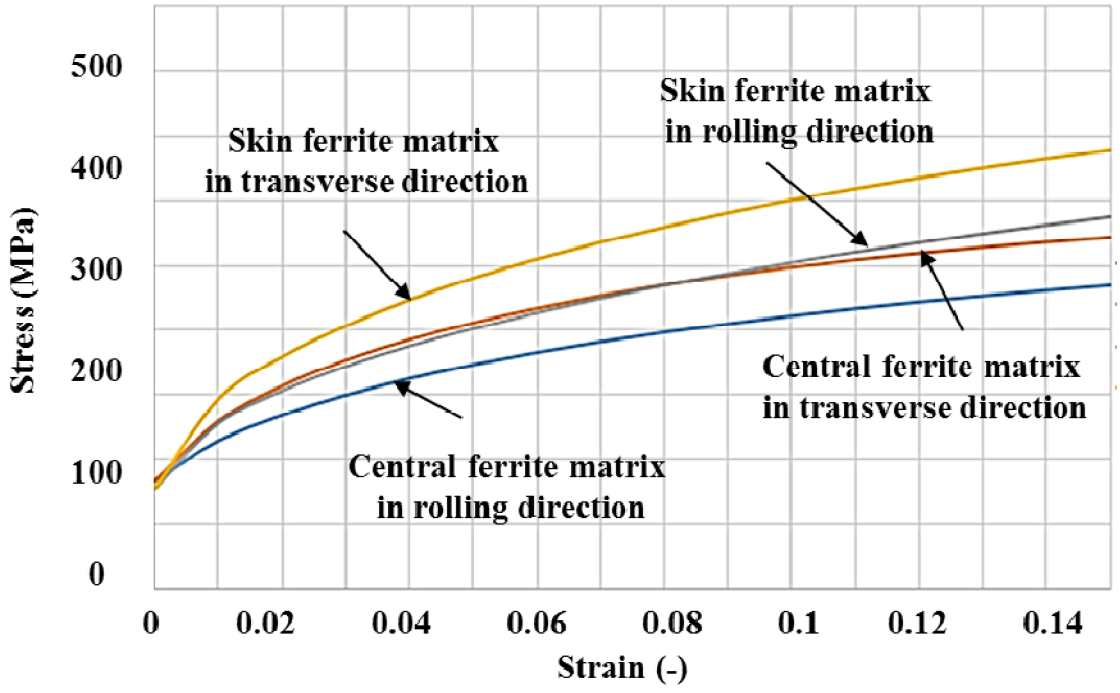

Figure 5. Predicted true stress–strain curves of ferrite matrix in the skin and central area of the examined steel.

Determination of effective flow stress of pipeline steel

For the micro–scale RVE, pearlites with different morphologies with stress–strain behavior obtained from the nano–scale calculations distributed in a ferritic matrix were generated, as shown in Figure 6a. Two micro–scale RVEs were examined, namely, RVE for the central area that consisted of 14.1% pearlitic and 85.9% ferritic phase fraction and RVE for the skin area that consisted of 13% pearlitic and 87% ferritic phase fraction. Moreover, two types of pearlite were defined in the RVEs, namely, elongated pearlite and prismatic pearlite with the phase fraction of 48.19% and 51.81%, respectively.[5] Orientations of the pearlite lamella were also taken into account, in which it was assumed to have pearlite lamella oriented in 0°, 45°, 90° and 135° with the volume fractions of 22, 31, 17 and 30%, respectively.[5] Subsequently, for obtaining effective properties of the X65 steel, virtual tensile tests were performed for the RVEs, as illustrated in Figure 6b. It was found that stress–strain curves of the X65 steel predicted by the micro–scale RVE model agreed well with experimental flow curves for both zones, as seen in Figure 7. Note that large deviations occurred at the strains between 0 and 0.04 because of the Lueders strain effects. However, it should be no effects on further analyses, since plastic strains, which were expected in pipe during the JCO forming process, were beyond this strain region.

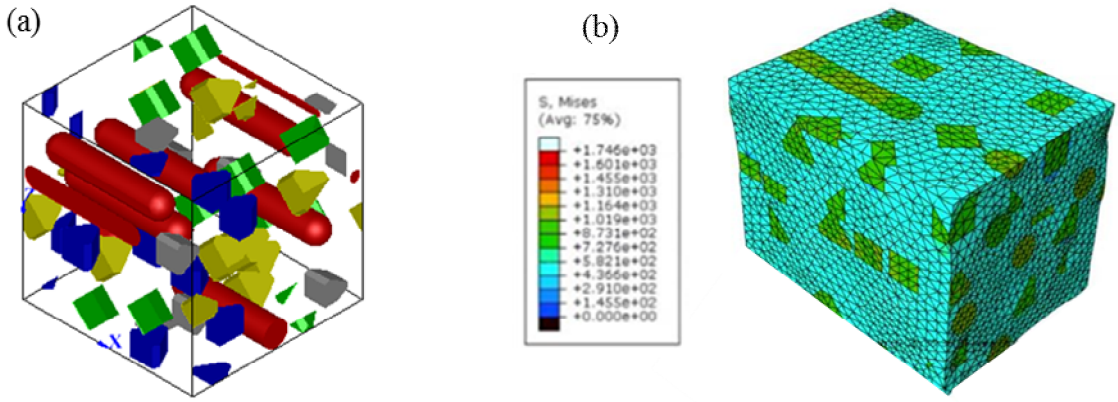

Figure 6. (a) Micro–scale RVE of microstructure of the investigated X65 steel and (b) calculated stress distributions of the RVE under tensile loading.

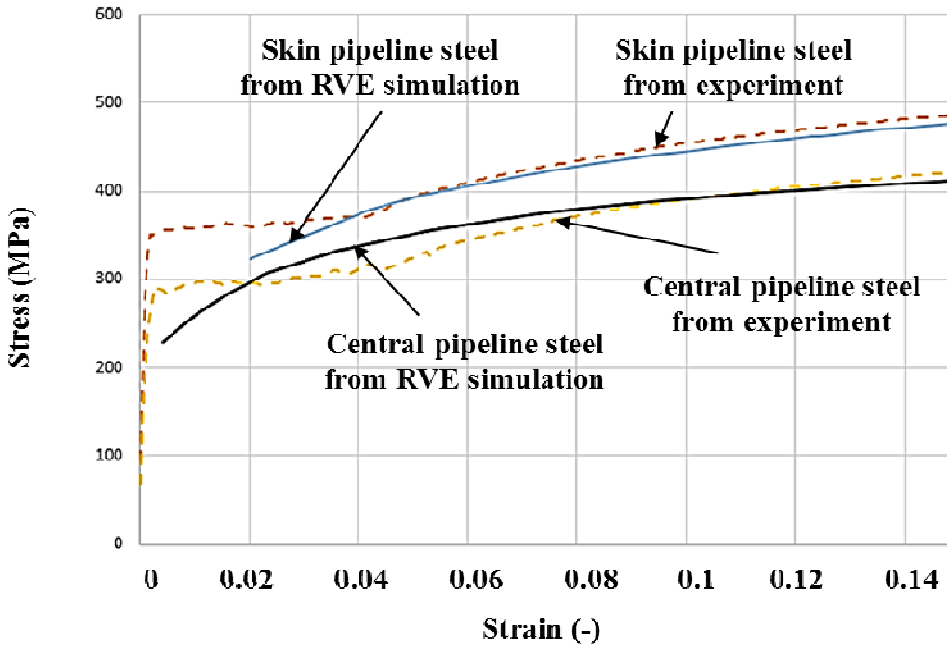

Figure 7. Comparison between flow stresses of the investigated X65 steel experimentally determined and calculated by RVE simulation.

JCO forming simulation of steel pipeline

Two FE simulations of the JCO forming were performed. By the first model (1–zone model), microstructure in the central area was assumed for the whole area of the tube. In case of the second model (2–zone model), different microstructures were incorporated in the skin and central area of the steel tube, in which2 layers of elements with the size of 1.58 mm x 2 were defined for both surfaces of the steel plate, as shown in Figure 8. Microstructures of each zone were described by applying the predicted flow curves for the skin and central area of the X65 steel plate. After that, JCO forming simulations were carried out for both models until reaching the final pipeline shape. FE models of the concerned JCO forming process consisted of die, pusher, support, which were defined as analytical rigid body, and steel plate, which was defined as a 2D deformable part, as illustrated in Figure 9. As a result, the most critical areas with the maximum stress on the formed tube were predicted by the 1– and 2–zone model, as shown in Figure 10. It can be observed that the maximum stress of the pipelinetube after forming occurred at the outer skin but at different positions in the 1–zone and 2–zonemodel. The maximum stresses of 482 MPa and 437 MPa were calculated by the 2– and 1–zone model, respectively. Considering different microstructures of the steel tube could significantly affect prediction of the critical area and following damaged site.

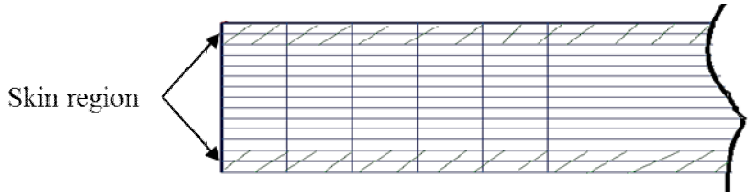

Figure 8. FE model of steel plate for defining different microstructures at the skin and central region (2–zone model).

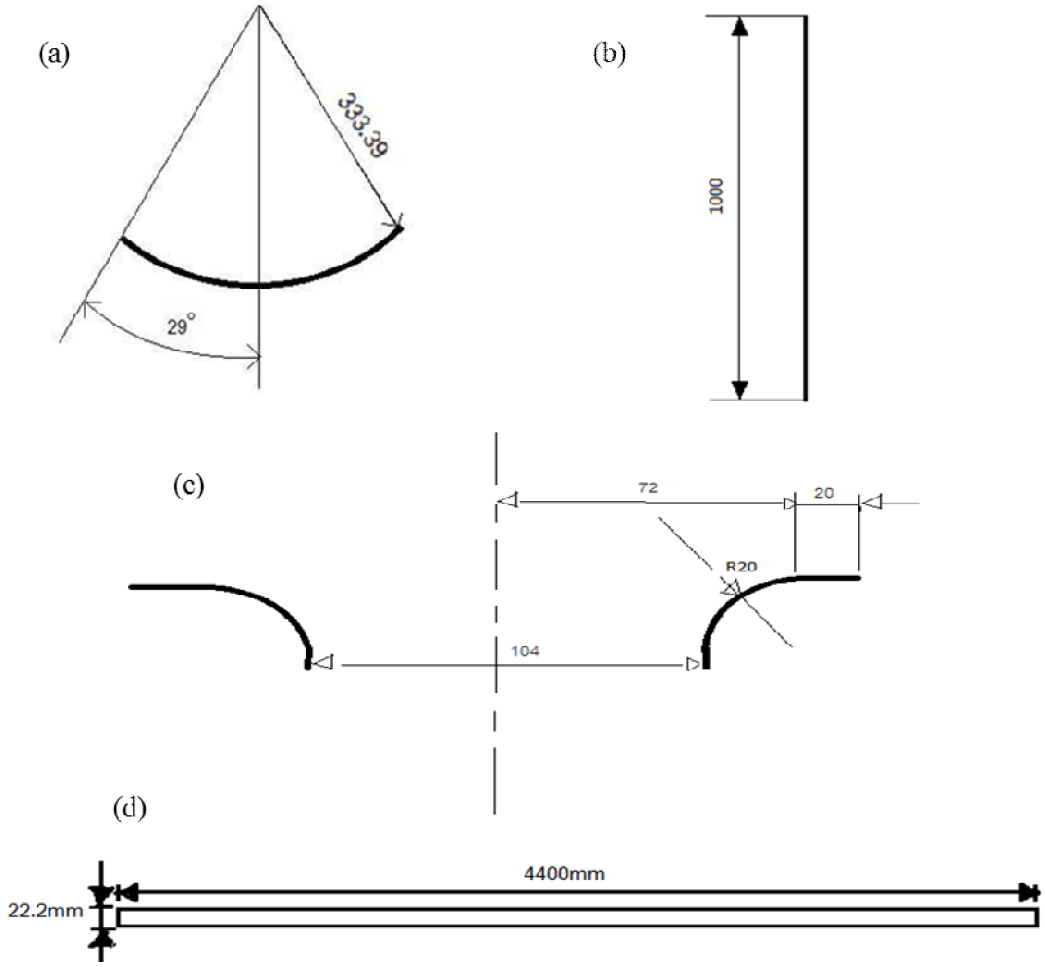

Figure 9. Geometries of FE models for (a) die, (b) pusher, (c) support and (d) steel plate in the JCO forming process.

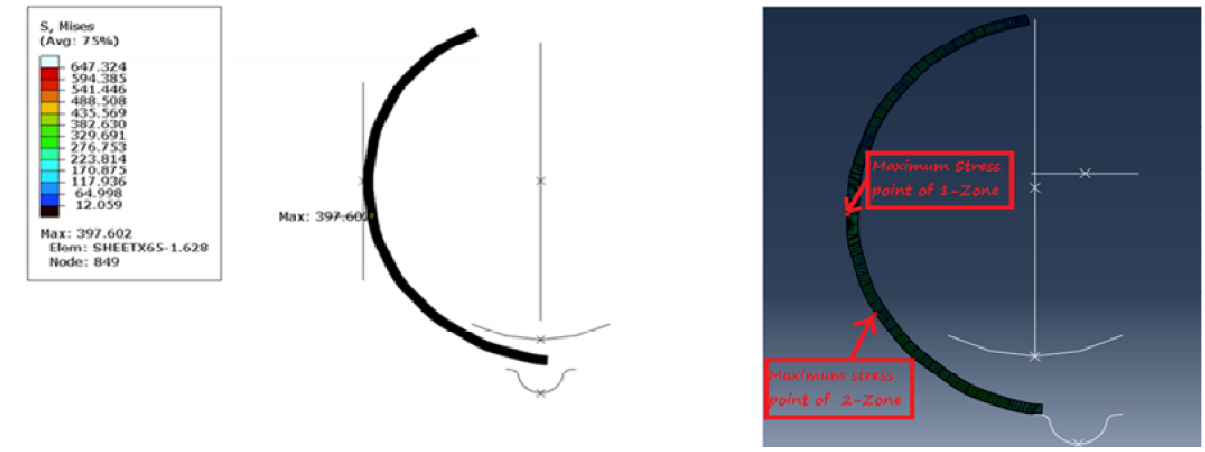

Figure 10. Most critical areas with the maximum stress on the formed tube predicted by the 1–zone and 2–zone model.

To verify the introduced approach, micro–scale RVE simulations were firstly carried out by applying deformation fields from the macroscopic tube forming simulation as boundary conditions and followed by uniaxial tensile loading. Note that both 1–zone and 2–zone models were considered. Figure 11 illustrated stress distributions of the deformed RVEs based on the 1–zone and 2–zone model after tube forming and tensile loading. Effective stress–strain responses from the RVE models were determined and compared with the experimental tensile test results of the pipeline steel grade X65 at the same region, as seen in Figure 12. It was found that flow curves obtained from both models were a little bit higher than that from the experiment at the beginning. On the other hand, predicted strain hardenings were lower than the actual one.

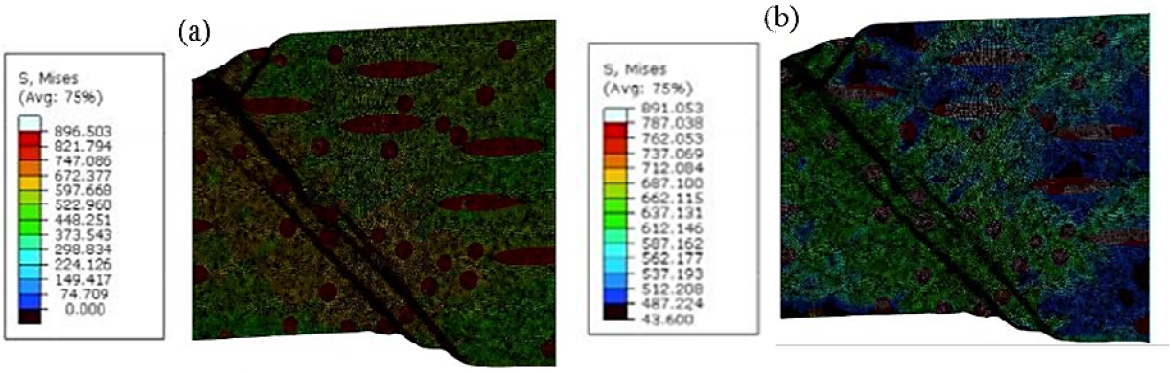

Figure 11. Calculated stress distributions of the RVEs after tube forming and tensile test for the (a) 1–zone model and (b) 2–zone model.

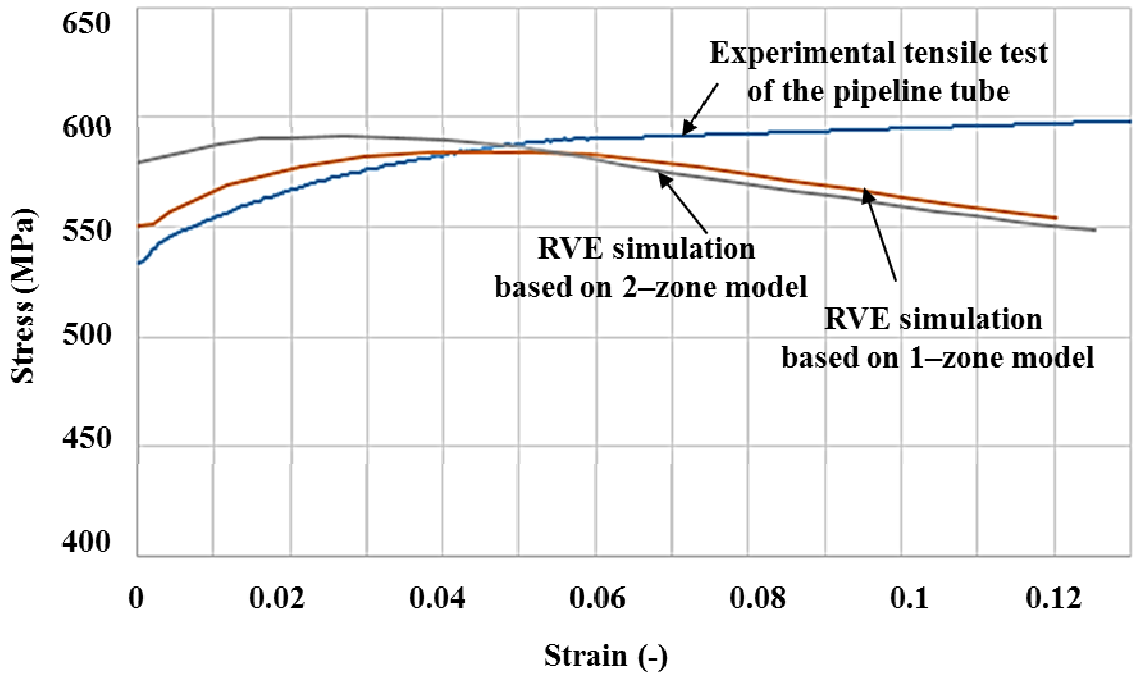

Figure 12. Comparison between stress–strain curves determined by experimental tensile test of the examined pipeline tube and calculated by the RVEs based on the 1–zone model and 2–zone model.

Finally, calculated deformation fields from the critical areas in the 1–zone and 2–zone models were taken and given as boundary conditions to the micro–scale RVEs for the central and skin microstructure, respectively. By this manner, local stress and strain distributions in the microstructure of the formed pipeline tube could be investigated. The deformed RVEs showed that the maximum stress of each model was observed at the harder pearlitic phase, as seen in Figure 13. The maximum stress of the RVE based on the 2–zone model was 796 MPa that was somewhat higher than that of the RVE based on the 1–zone model. This local critical stress value is rather larger than that obtained from the macro–scale model.

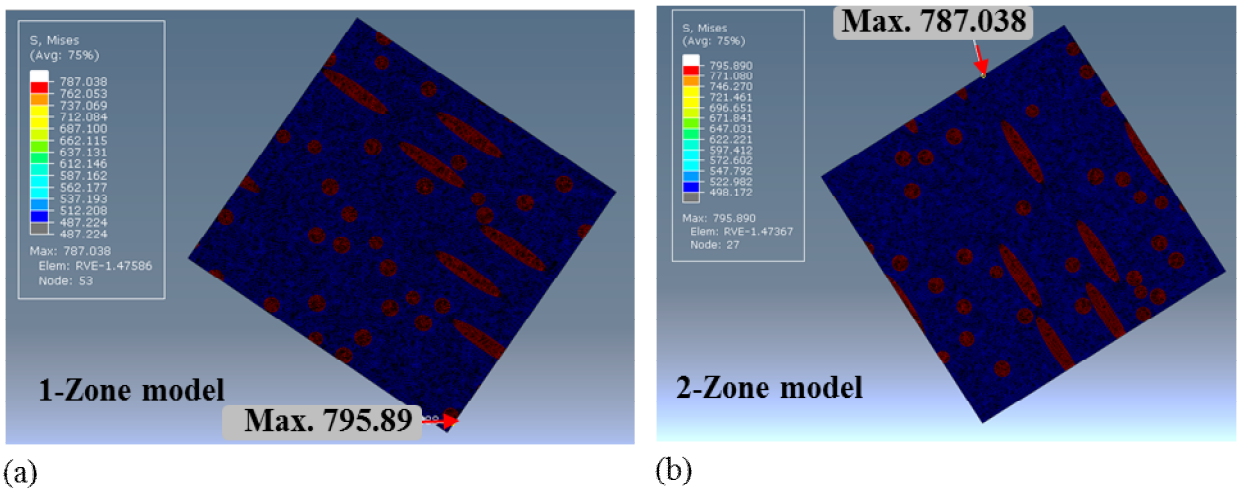

Figure 13. Calculated local critical areas in the microstructure of formed pipeline tube based on the (a) 1–zone model and (b) 2–zone model.

Conclusions

In this work, multi–scale modeling approach for determining flow stress behavior of the pipeline steel tube grade X65 was introduced. Different microstructure characteristics of surface and central area of the tube due to unlike cooling rate by hot rolling process were taken into account. Effective stress–strain curves and anisotropy yield stress ratios of pearlite were determined by the bi–lamella RVE simulations. Then, stress–strain curves of the steel tube were obtained by macro–scale RVE simulations, for which anisotropic yield behavior was defined for the pearlite with various configurations and ferrite matrix. The results for both zones were comparable with the ones from tensile tests. Macroscopic simulations of the JCO forming were carried out by using effective properties derived from the RVE calculations. Critical areas of the formed tube were then investigated. The main findings of this work could be drawn as following.

– By calculation at the nano–scale, flow stresses in the *xx* and *yy* direction of pearlite in the skin area were similar, while flow stresses in the *yy* and *zz* direction were similar in the central zone of the pipeline tube. The strain hardenings of pearlite in both zones were identic.

– Different cooling rates of the skin and central areas significantly affected flow stress behavior of the steel pipe.

– The critical location on the tube after JCO process occurred on the surface area between left and bottom side.

– The macroscopic maximum stress obtained from by the 2–zone model was higher than that from the 1–zone model.

– Local maximum stress in the microstructure of pipeline tube after forming determined by RVE based on the 2–zone model was higher than that from the 1–zone model because of finer ferritic grain and smaller lamellar spacing at the skin area. However, the maximum stresses occurred at the hard pearlitic phase in both RVE models.

Acknowledgment

The authors would like to acknowledge Office of the Higher Education Commission, Thailand Research Fund (TRF) and King Mongkut's University of Technology Thonburi (KMUTT) for financial supports (TRG5880258).

References

1. PTT Public Company Limited. (2555). *Natural gas everyday*. PTT Public Company Limited, Bangkok.

2. Wang, J. Q., Atrens, A., Cousens, D. R. and Kinaev, N. (1999). Microstructure of X52 and X65 pipeline steels. *J. Mater. Sci.* **34(8)** : 1721-1728.

3. Allain, S. and Bouaziz, O. (2008). Microstructure based modeling for the mechanical behavior of ferrite-pearlite steels suitable to capture isotropic and kinematic hardening. *Mater. Sci. Eng. A.* : **496(1-2)** : 329-336.

4. Laschet, G., Fayek, P., Henke, T., Quade, H. and Prahl, U. (2013). Derivation of anisotropic flow curves of ferrite–pearlite pipeline steel via a two–level homogenization scheme. *Mater. Sci. Eng. A.* **566** : 143-156.

5. Laschet, G., Shukla, M., Henke, T., Fayek, P., Bambach, M. and Prahl, U. (2014). Impact of the microstructure on the U-O forming simulations of a ferrite-pearlite pipeline tube. *Steel Res. Int.* **6** : 1083-1098.

6. Palumbo, G. and Tricarico, L. (2005). Effect of forming and calibration operations on the final shape of large diameter welded tubes. *J. Mater. Proc. Technol.* **164-165** : 1089-1098.

7. Ren, Q., Zon, T., Li, D., Tang, D. and Peng, Y. (2015). Numerical study on the X80 UOE pipe forming process. *J. Mater. Proc. Technol.* **215** : 264-277.

8. Liu, P. F., Zheng, J. Y., Zhang, B. J. and Shi, P. (2010). Failure analysis of natural gas buried X65 steel pipeline under deflection load using finite element method. *Mater. Des.* **31(3)** : 1384-1391.

9. Gutierrez, I. and Altuna, M. A. (2008). Work-hardening of ferrite and microstructure-based modeling of its mechanical behavior under tension. *Acta Materialia.* **56** : 4682-4690.

10. Sirinakorn, T., Wongwises, S. and Uthaisangsuk, V. (2014). A study of local deformation and damage of dual phase steel. *Mater. Des.* **64** : 729-742.

11. Hagi, H. (1994). Effect of interface between cementite and ferrite on diffusion of hydrogen in carbon steel. *Mater. Trans. JIM.* **35(3)** : 168-173.

12. Keller, C., Hug, E., Habraken, A. M. and Duchene, L. (2012). Finite element analysis of the free surface effects on the mechanical behaviour of thin nickel polycrystals. *Int. J. Plasticity.* **29** : 155-172.

13. Hangen, U. (2010). *Mechanical properties of multi–phase materials*. Hysitron Inc., USA.